Unveiling the Mechanisms Governing the Exchange Coupling and Coercivity Modifications in Annealed or Ion-Irradiated Ir-Mn/Fe/Co and Ir-Mn/Ni-Fe/Co films

J.B. Salazar,[1] L.G. Pereira,[1] P L. Grande,[1] J.E. Schmidt,[1] J.A. Schneider,[1] S. Nicolodi,[1] V. Skumryev,[2,3] A. Harres,[4] P. Steadman,[5] P. Bencok,[5] A. Dobrynin,[6] and J. Geshev[1,*]

[1] *Instituto de Física, URFGS, Porto Alegre, Rio Grande do Sul, 91501-970, Brazil*
[2] *Departament de Física, Universitat Autònoma de Barcelona, 08193 Barcelona, Spain*
[3] *Institució Catalana de Recerca i Estudis Avançats, 08010 Barcelona, Spain*
[4] *Departamento de Física, UFSM, Santa Maria, Rio Grande do Sul, 97105-900, Brazil*
[5] *Diamond Light Source, Harwell Science and Innovation Complex, Didcot, OX11 0DE, United Kingdom*
[6] *Seagate Technology, 1 Disc Drive, Derry, BT48 0BF, United Kingdom*

(Received 7 June 2018; revised manuscript received 3 September 2018; published 10 December 2018)

We investigate the modifications of the exchange bias, effective ferromagnet-antiferromagnet (FM-AFM) coupling, and coercivity in annealed or ion-irradiated Ir-Mn/spacer layer (SL)/Co trilayers. A ferromagnetic, either Fe or permalloy (Py), thin SL or a nonmagnetic Ru one with different thicknesses (t_{SL}) is used. The magnetic characterization is performed at room temperature via conventional magnetometry and, partly, via soft-x-ray magnetic circular dichroism. The latter shows that at the FM-AFM interface there is small uncompensated Mn magnetization coupled, preferentially, antiferromagnetically to Fe moments. This indicates the formation of small FeMn clusters that reverse their magnetizations together with those of Co, Ni, and the rest of Fe. Neither annealing nor ion irradiation of the films with $t_{Fe} \geq 0.5$ nm changes significantly the pinning part of the FM-AFM interface. In the Py-spacer films, however, the great tendency of Mn to interdiffuse with Ni leads to a decrease of the Ir-Mn anisotropy at the interface, lowering its pinning capacity. While defects created in the bulk of the AFM are mainly responsible for the changes of the magnetic characteristics of the Ir-Mn/Fe/Co films, interdiffusion and defect creation at the FM-AFM interface are the respective mechanisms determining the behavior of the Py-spacer series. These conclusions are reinforced by results for the Ru-spacer series.

DOI: 10.1103/PhysRevApplied.10.064021

I. INTRODUCTION

The magnetic exchange-bias (EB) phenomenon [1] results from exchange coupling between a ferromagnet (FM) and uncompensated spins (UCSs) at the interfacial region of a magnetic material, normally an antiferromagnet (AFM). Its best-known manifestation is the hysteresis-loop shift along the magnetic field (H) axis referred to as the "EB field" (H_{EB}). The EB, widely studied in recent decades and already used in magnetoelectronic devices, is still being intensively investigated given the advent of new production technologies, powerful experimental techniques, and increasingly-more-complex magnetic systems. Usually, EB is set by application of a magnetic field during the sample's production or by cooling it down through the Néel temperature (T_N). One can also initialize EB by post-deposition ion bombardment (IB) [2–4] in a magnetic field or by application of sufficiently large magnetic fieldsat a fixed temperature [5]; the FM remnant magnetization acquired before cooling [6] can also set the effect.

The interfacial UCSs play a key role in EB systems. The model of Fulcomer and Charap [7] served as a basis for most of the granular EB systems and considers the effects of the UCS grain-size distribution at FM-AFM interfaces. It is now accepted that the UCSs can be divided into four categories [8–11]: (i) Superparamagnetic UCSs, which are thermally unstable during the measurement and do not contribute to either H_{EB} or coercivity (H_C) (i.e., half width of the hysteresis loop). (ii) *Partially stable* UCSs, which may rotate together with the FM's magnetization, resulting in H_C enhancement and rotatable anisotropy [12–15]. (iii) *Set* UCSs (i.e., the ones preferentially aligned along **H** present during the preparation or post-treatment of the sample), which are responsible for the bias. (iv) *Unset* UCSs, which cannot be reversed through the postproduction treatment. However, a highly anisotropic UCS could contribute to H_C but not to H_{EB} if the coupling with the FM is strong enough, while a weakly coupled low-anisotropy UCS could add to the bias [16,17].

*julian@if.ufrgs.br

One can manipulate the strength of the exchange coupling (J) between magnetic layers by introducing a nonmagnetic (either conductor or insulator) spacer layer (SL) at their interface [15,18–22]. In bottom-pinned EB films, where the FM is grown onto the pinning AFM, the introduction of such a SL leads to a decrease of the bias. The only exception seems to be an ultrathin SL of Mn, which is shown to cause EB enhancement in Ir-Mn/Co-Fe and Ir-Mn/Co_2FeSi polycrystalline films [23,24]. In top-pinned systems, where the FM is pinned via UCSs at the interface with the AFM grown on top of it, the insertion of a Pt spacer in $(Pt/Co)_3$/Pt/Ir-Mn multilayers seems to limit the Mn and Ir diffusion in the Co layer [25]. It has been found that the biasing can be enhanced by the introduction of a *ferromagnetic* spacer at the FM-AFM interface in top-pinned Co/SL(Ni)/Ir-Mn, Co/SL(Fe)/Ir-Mn, and Co/SL[permalloy (Py)]/Ir-Mn films [18], where it has been suggested that the EB increase is related to an inhomogeneous magnetic interface.

Industrially, Ir-Mn is the mostly used AFM due to its good corrosion endurance, high anisotropy, and high blocking temperature as well as small critical thickness to establish EB. It also exhibits a high spin Hall angle, so it is a good converter of spin currents into charge currents and an excellent candidate for spintronics applications [26].

Here we present modifications of H_{EB}, H_C, and the interface coupling after either annealing or IB of Ir-Mn/SL/Co films (SL is Fe, Py, or Ru). Each SL is considered as an impurity layer, and the main goal of the study is to determine how it affects the EB parameters. The mechanisms determining their variations are discussed. We obtain that while defects (i.e., interstitial atoms and vacancies) created in the bulk of the AFM are mainly responsible for the changes of the magnetic characteristics of the Ir-Mn/Fe/Co films, the mechanisms determining the properties of the Py-spacer series are interdiffusion and defect creation at the FM-AFM interface.

II. EXPERIMENTAL

Three different series of Ir-Mn(7 nm)/SL/Co(5 nm) trilayers are grown at room temperature onto Si(100)/Ta(5 nm)/Ru(15 nm), where the nonmagnetic Ta/Ru bilayers are deposited to induce the Ir-Mn(111) texture required for bias. To avoid oxidation, each film is covered by a 3-nm-thick Ru cap layer. The films of the first set (i.e., Si/Ta/Ru/Ir-Mn/Py/Co/Ru) are referred to as Ir-Mn/Py/Co; those with an Fe SL (i.e., Si/Ta/Ru/Ir-Mn/Fe/Co/Ru) are referred to as Ir-Mn/Fe/Co, and the films of the third series with a Ru SL (i.e., Si/Ta/Ru/Ir-Mn/Ru/Co/Ru) are referred to as Ir-Mn/Ru/Co. The SL thicknesses, t_{Py}, t_{Fe}, and t_{Ru}, are varied from 0.25 to 1.50 nm. The samples are grown by magnetron sputtering from Ta, Ru, Fe, Py (i.e., $Ni_{81}Fe_{19}$), Co, and $Ir_{20}Mn_{80}$ targets (base pressure 5.0×10^{-8} mbar, Ar pressure 2.5×10^{-3} mbar for the deposition of Ta, Ru, Fe, Py, and Co, and 1.0×10^{-2} mbar for deposition of Ir-Mn).

The structural characterization of the films is done at room temperature by conventional x-ray diffractometry in a θ-2θ Bragg-Brentano geometry with Cu K_α radiation.

The magnetic measurements are performed at room temperature with an alternating-gradient force magnetometer (AGFM) with maximum magnetic field of 3 kOe applied in the plane of the films. The magnitude of this field is sufficiently high to avoid EB overestimation due to minor-loop effects [27,28] for all samples. We also ensure that the data are collected after time intervals sufficiently long to avoid temporal changes of H_{EB}; that is, the so-called thermal-drift effect [29]. For a number of films, in-plane-magnetization (M) hysteresis loops are also measured with a MicroSense EZ9 vibrating-sample magnetometer.

In all measurements and for each sample, the hard direction is first determined (i.e., the one for which the magnetization curve is unshifted and symmetric through the origin). Then the easy-axis hysteresis loop, corresponding to a direction 90° from the hard one, is traced. Since even a small misalignment might result in a great H_C variation, measurements for **H** applied ±3° from the predetermined easy-axis direction are performed to ensure that this loop shows a maximum H_C value and, finally, two more loops are measured; no appreciable training effect is observed for any of the samples.

After determination, by use of the AGFM, of the EB direction induced by the magnetron field during deposition, pieces of all films are subjected to annealing in an electric resistive furnace with a magnetic field of 2.1 kOe applied along this direction. Each sample is kept at 210 °C for 15 min and then cooled to room temperature in a vacuum (pressure of less than 10^{-6} mbar). A piece of as-made Ir-Mn/Py(0.5 nm)/Co film is annealed at 150 °C instead of 210 °C, and exhibits a slightly lower EB value. Samples of all series are also submitted to He^+ IB at 40 keV in a vacuum, with a current of 100 nA/cm^2 and fluences ranging from 5×10^{13} to 1×10^{16} ions/cm^2, in the presence of an in-plane magnetic field of 5.5 kOe applied along the sputtering-induced EB direction.

Soft-x-ray magnetic circular dichroism (XMCD) measurements are performed at the I10 beamline at the Diamond Light Source on the Ir-Mn/Py(0.5 nm)/Co film annealed at 150 °C to obtain information on the magnetic behavior of Co, Ni, Fe, and Mn at the FM-AFM interface. Element-specific hysteresis loops are traced by our measuring XMCD at the peak values for Co, Fe, and Ni L_2 and L_3 edges as a function of H. The measurements are conducted with the sample positioned at 10° with respect to directions of both the incident beam and the applied magnetic field, as close as possible to the sample's easy direction. The maximum H value of 500 Oe for these measurements ensures saturation of the samples.

III. RESULTS AND DISCUSSION

A. Structural properties

The x-ray-diffraction analysis identifies high ⟨111⟩ texturing of the Ir-Mn and Co layers, promoted by the Ru buffer. Peaks corresponding to the Py or Fe spacer are not detectable owing to their small thicknesses. The position of the Ir-Mn(111) peak does not change with the insertion of the SLs. The Co(111) peak, however, gets progressively weaker with the increase of the SL's thickness (t_{SL}) for each spacer, indicating that with SL insertion at the Ir-Mn/Co interface, the Co growth orientation gradually loses the pattern induced by Ir-Mn.

B. Magnetization curves

Magnetization hysteresis loops, measured along the easy and hard magnetization directions for the Ir-Mn/Co bilayer and for the Ir-Mn/Py/Co and Ir-Mn/Fe/Co films before and after the magnetic annealing are plotted in Fig. 1. Each curve, corresponding to an as-made film, is composed of two well-defined subloops. The weak magnetron stray field, present during the deposition, has disturbed the interfacial AFM spin balance, resulting in a small loop shift. Representative loops, measured after either annealing or IB, are also plotted in Fig. 1, and demonstrate that each postdeposition treatment results in well-defined rectangular easy-axis loops, shifted along the field axis.

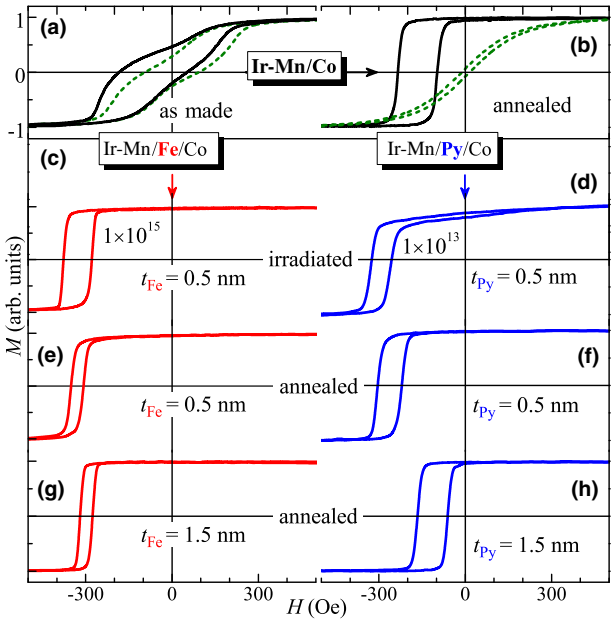

FIG. 1. Hysteresis loops measured along the easy (full lines) and hard (dashed lines) axes for the Ir-Mn/Co bilayer before (a) and after (b) annealing. Easy-axis curves traced after IB (with fluences of 1×10^{15} and 1×10^{13} ions/cm^2 for $t_{Fe} = 0.5$ nm and $t_{Py} = 0.5$ nm, respectively) are shown in (c),(d). Representative easy-axis loops for annealed Ir-Mn/Fe/Co and Ir-Mn/Py/Co films are plotted in (e)–(h).

The curves measured along the respective hard directions exhibit continuous $M(H)$ variations and very small coercive fields.

Although the key role of interfacial UCSs for EB seems well established, questions concerning their origin still remain. For example, while in Ir-Mn/Co-Fe films O'Grady *et al.* [30] attributed the UCSs to AFM spins, Berkowitz *et al.* [31] found strong indications that, as a result of chemical reactions at the interfaces of their Py/CoO bilayers, there are hard particles coupled to the CoO. Here we try to clarify whether some atoms of the magnetically softer SL, if strongly coupled to the adjacent set-type UCSs, do not rotate with the rest of the FM, which would result in a shift along the M axis. Since the AGFM measurements performed do not allow quantitative estimation of the magnetization, $M(H)$ (not shown) is measured with a vibrating-sample magnetometer for samples with $t_{Py} =$ 0.5, 1.0, and 1.5 nm. None of these loops exhibits a shift along the M axis, and the respective H_{EB} values are practically the same as the AGFM-estimated ones.

C. Soft-x-ray magnetic circular dichroism results

The XMCD spectra of the Ir-Mn/Py(0.5 nm)/Co film annealed at 150 °C measured at a saturation field of 500 Oe at Co, Fe, Ni, and Mn $L_{2/3}$ absorption edges by total fluorescence yield are given in Fig. 2. The spectra are measured across both the L_3 edge and the L_2 edge first for right circular polarization, and then for left circular polarization provided by versatile I10's APPLE-II insertion devices [32]. According to the standard convention, "right" circular polarization is defined with the

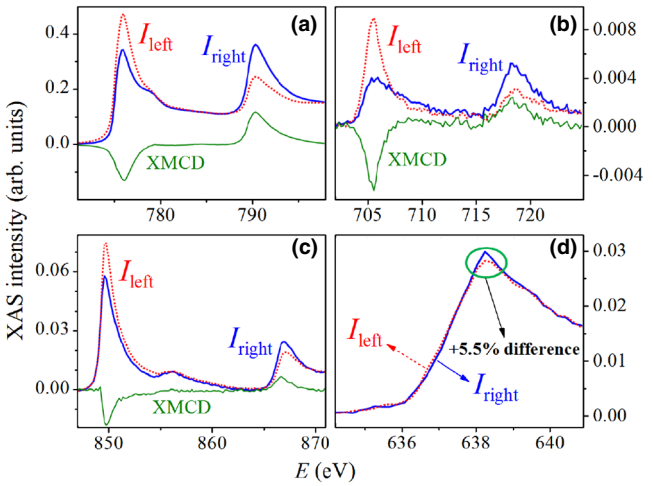

FIG. 2. X-ray absorption spectra (XAS) from an Ir-Mn/Py(0.5 nm)/Co film annealed at 150 °C measured across the L_3 and L_2 edges of Co (a), Ni (b), Fe (c), and Mn (d) (enlargement for L_3 edge only) in in-plane geometry along the easy axis at 500 Oe. A small positive XMCD signal is evident from (d), implying the existence of AFM UCSs and their antiparallel orientation to Co, Ni, and Fe magnetizations.

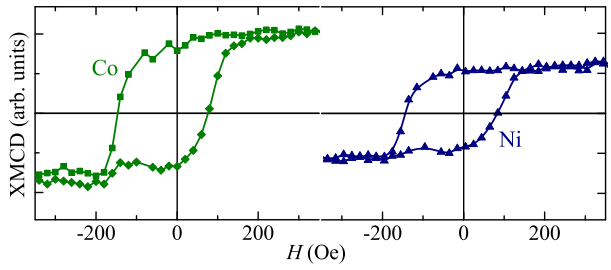

FIG. 3. Element-specific hysteresis loops for the Ir-Mn/Py(0.5 nm)/Co film annealed at 150 °C obtained by measurement of peak XMCD signals at the Co and Ni L_3 edges as a function of H. The lines are only guides for the eye.

incident-beam electric field vector **E** rotating clockwise when one is looking from the source, and "left" circular polarization corresponds to **E** rotating counterclockwise. The magnetic field is applied in the direction of the beam's propagation. The XMCD signal at the L_3 edge is positive for Co, Ni, and Fe [Figs. 2(a)–2(c)]. However, for the Mn L_3 edge there is a small positive XMCD signal as can be seen from the enlargement shown in Fig. 2(d). This means that (i) there is a small uncompensated Mn magnetization and (ii) it couples antiferromagnetically to the FM film. It is well known that while Mn couples antiferromagnetically to Fe, it couples ferromagnetically to Co and Ni [26,33]. The observation of antiferromagnetic interface coupling means a preferential coupling of Mn to Fe, in spite of the lower concentration at the interface of Fe (19%) as compared with Ni (81%). This suggests the formation of small FeMn clusters at the interface. The element-specific hysteresis loops (Fig. 3) of the Co and Ni L_3 edges confirm their simultaneous reversal. Although no such loops are recorded for Mn or Fe due to high noise levels, it seems reasonable to assume that Fe and possibly FeMn clusters reverse their moments together with those of Co and Ni, as no shift along the M axis is observed in our vibrating-sample-magnetometer measurements.

D. Exchange bias and coercivity versus SL thickness

The variations of H_{EB} and H_C with the SL material, with t_{SL}, and with the postdeposition treatment method give valuable information on the effective coupling strength (J_{eff}). For weak (as compared with the anisotropy of the set-type UCSs) coupling, the simple expression

$$J_{eff} = H_{EB}(M_S^{Co} t_{Co} + M_S^{SL} t_{SL}) \qquad (1)$$

is expected to hold [18,34], where M_S refers to the saturation magnetization. Normally, J_{eff} is orders of magnitude smaller than J of an ideal system since only a small fraction of the interface contributes to H_{EB}. Thus $J_{eff} \propto \rho J$, ρ being the nominal thickness of the pinned uncompensated layer in fractions of a monolayer [35]; ρ can also be interpreted as the number, n_{set}, of set-type UCSs in fractions of

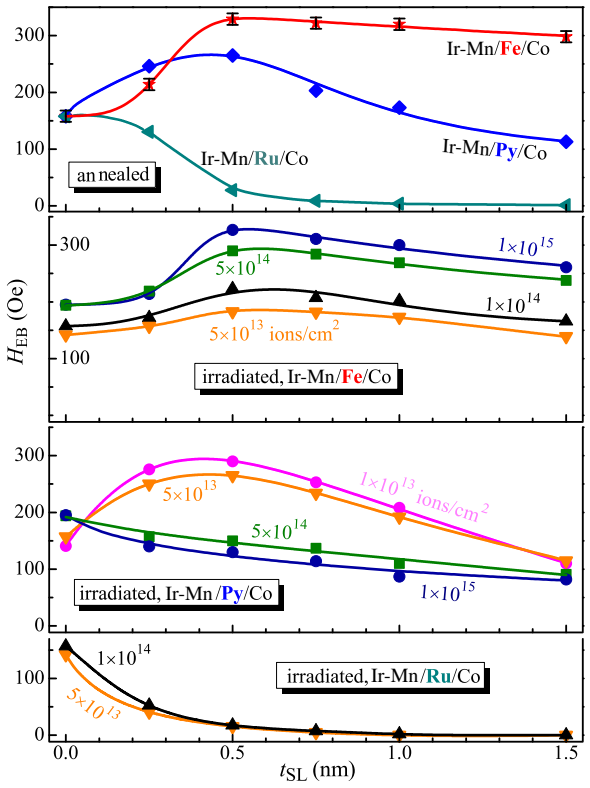

FIG. 4. H_{EB} versus t_{SL} (SL is Fe, Py, or Ru) for annealed and ion-irradiated (with different fluences) Ir-Mn/SL/Co films. The length (±10 Oe at most) of the error bars is of the size of the data symbols, exemplified for the topmost data (annealed Ir-Mn/Fe/Co). The lines are only guides for the eye. The same symbols and line types, identifying the SL material and/or treatment (annealing or IB fluence), are used in Fig. 5.

the total number, n, of UCSs (i.e., $0 \leq n_{set} \leq 1$). Also, the higher the degree of alignment of the UCSs with the EB direction, the bigger J_{eff} is. Likewise, one can define n_{rot} as the number, in fractions of n, of the UCSs responsible for the coercivity enhancement.

The dependencies of H_{EB} on t_{SL}, extracted from the easy-axis hysteresis loops of annealed and ion-irradiated samples, are given in Fig. 4. The Ru-spacer curves show a monotonous decay due to the gradual reduction of J_{eff} with t_{Ru} normally expected for nonmagnetic SLs. Almost all $H_{EB}(t_{Fe})$ and $H_{EB}(t_{Py})$ variations, however, exhibit a significant initial rise up to $t_{SL} \approx 0.5$ nm, followed by a monotonous decrease, the exception being the ion-irradiated Ir-Mn/Py/Co samples when the two highest fluences are used. The gradual reduction of H_{EB} of the latter comes, most probably, from the extensive damage caused by high-fluence IB at the FM-AFM interface.

According to Eq. (1), one would expect a monotonous *decay* of H_{EB} with t_{SL} for the series with FM spacers. Thus, the observed initial *rise* of $H_{EB}(t_{SL})$ for Fe and Py SLs is attributed to an enhancement of $J_{Ir\text{-}Mn/SL}$ due the increase of the Ir-Mn/SL contact area at dispense of the

Ir-Mn/Co contact area. Given that the $J_{\text{Ir-Mn/Fe}}$ and $J_{\text{Ir-Mn/Py}}$ values are both greater than $J_{\text{Ir-Mn/Co}}$ [36,37], J_{eff} rises and so does H_{EB}. The subsequent decrease of H_{EB} for $t_{\text{SL}} > 0.5$ nm can be understood by our considering that $t_{\text{SL}} \approx 0.5$ nm is the point at which the SL atoms cover practically all set-type UCSs, so J_{eff} has attained its maximum value and any further rise of t_{SL} would only result in decreasing $H_{\text{EB}} \propto 1/t_{\text{SL}}$.

The variations of the easy-axis H_C with t_{SL} are given in Fig. 5. The coercivity of the annealed samples shows a general trend of decrease for all FM spacers. In general, each $H_C(t_{\text{SL}})$ of the irradiated FM-spacer samples attains a maximum at t_{SL} lower than that maximizing H_{EB}; the values of H_C obtained after IB are, in general, greater than those obtained after annealing, and the higher the position of the $H_{\text{EB}}(t_{\text{SL}})$ curve in the graph, the lower the corresponding position of $H_C(t_{\text{SL}})$ is. Moreover, the $H_C(t_{\text{Py}})$ curves when the two lowest fluences are used are qualitatively similar to those obtained after annealing. The cause of the initial H_C enhancement for $t_{\text{SL}} \leq 0.25$ nm, observed for most of the irradiated FM-spacer samples, seems to be the one leading to the initial increase of H_{EB} (i.e., a rise of J_{eff} as the SL/Ir-Mn contact area is increased. The subsequent gradual decrease with t_{FM} $(= t_{\text{Co}} + t_{\text{SL}})$ agrees with both theory and experiment; namely, $H_C \propto 1/t_{\text{FM}}^k$ for k between 1 and 2 [38–40].

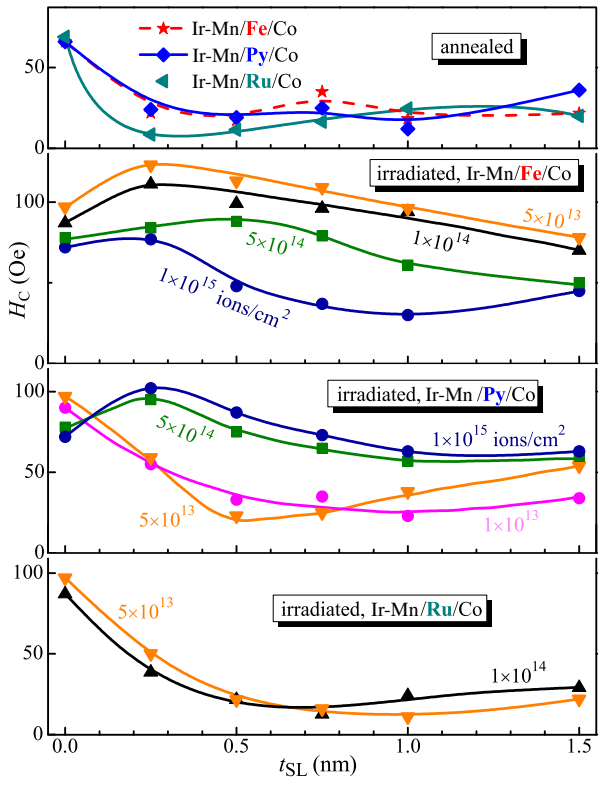

FIG. 5. H_C versus t_{SL} for annealed and ion-irradiated Ir-Mn/SL/Co films. The length of error bars is of the size of the data symbols.

E. Interface coupling and coercivity versus IB fluence

Important insights into the mechanisms responsible for the bias and coercivity variations of the FM-spacer films are obtained by our examining the dependencies of J_{eff} [estimated from Eq. (1)] and H_C on the IB fluence plotted in Figs. 6 and 7. These, rather differently from $H_{\text{EB}}(t_{\text{SL}})$ and $H_C(t_{\text{SL}})$, show monotonous variations only. As the great majority of our magnetization measurements are performed with an AGFM, which does not allow one to obtain the value of M, the literature M_S values of Co, Fe, and Py are used (1400, 1700, and 780 emu/cm^3, respectively) when we are estimating J_{eff} through Eq. (1). It is well known that up to a certain thickness, M_S may increase with increasing FM thickness, which influences the estimated values of J_{eff}, as discussed in Sec. III F.

It is well established that in EB systems IB supplies energy for spin rearrangement and may lead to EB modifications [29,41,42] by (i) local hyperthermal energy transfer of ions, (ii) defect (interstitial atoms and vacancies) creation in the AFM, and (iii) FM-AFM interface intermixing. The first mechanism acts in a manner very similar to annealing, supplying energy for aligning some of the UCSs with **H**, thus increasing H_{EB} [29]. Usually, the major increase of H_{EB} through IB is attributed to the creation of interstitial atoms and vacancies in the AFM [10]. Namely, nuclear energy losses of the impinging ions [4,43] in the bulk of the AFM reduce its anisotropy, resulting in an increase of n_{set} and a decrease of n_{rot} if no new UCSs are created. On the other hand, defects created at the FM-AFM interface decrease J_{eff} due to broken exchange bonds across

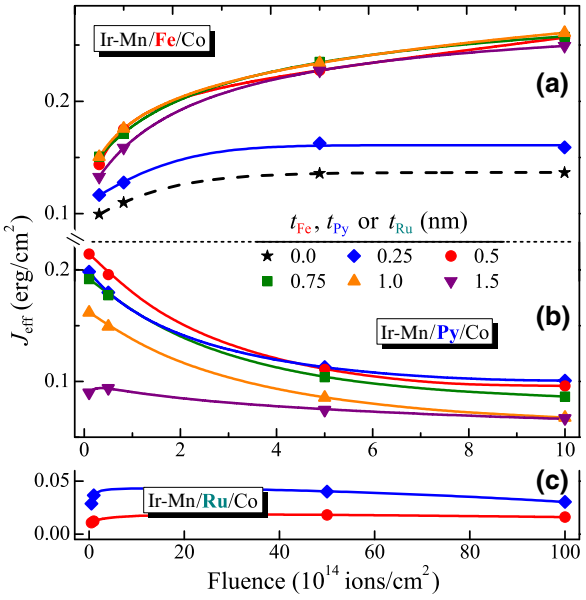

FIG. 6. J_{eff}, estimated from Eq. (1), versus IB fluence for the Ir-Mn/SL/Co films. The error bars are of the size of the data symbols, and the lines are guides for the eye. The same symbols and line types, identifying the SL's thickness, are used in Fig. 7.

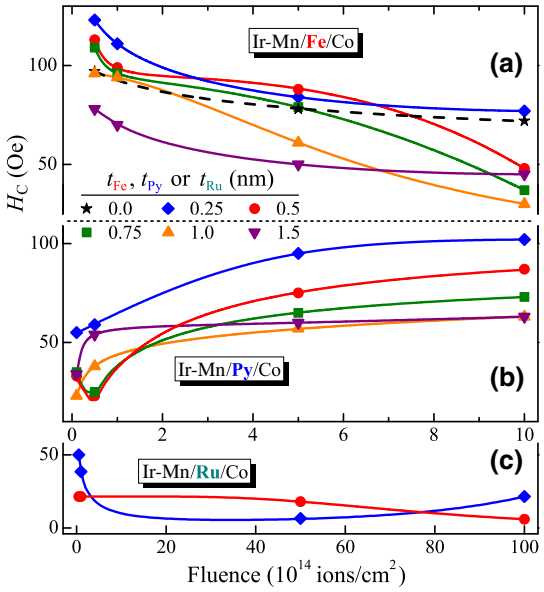

FIG. 7. H_C versus IB fluence for Ir-Mn/SL/Co films. The length of the error bars is of the size of the data symbols.

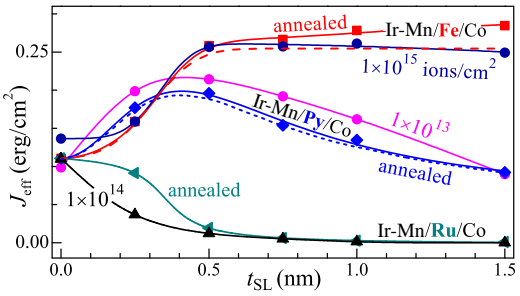

FIG. 8. $J_{eff}(t_{SL})$ estimated from Eq. (1) for annealed and ion-irradiated Ir-Mn/SL/Co. The error bars are shorter than the size of the data symbols. The long and short dashed lines give the variations of $J_{eff}(t_{Fe})$ and $J_{eff}(t_{Py})$, respectively, estimated for the annealed series assuming a linear increase of M_S, from 0 to 60% of the respective literature values.

the interface and, consequently, the bias. For high fluences, the decrease in n_{set} could be more drastic and may outweigh the effect of decreasing AFM anisotropy constant, so interfacial defects may become important. It has recently been estimated that kiloelectronvolt He^+ IB of polycrystalline Ir-Mn/$Co_{70}Fe_{30}$ films has a stronger impact on the magnetic characteristics of smaller interface grains with UCSs as compared to those of larger ones, reducing their rotatable anisotropy [44].

Thus, as for Ir-Mn/Co films [10], the gradual rise of J_{eff} and decay of H_C for moderate fluences of the Ir-Mn/Fe/Co films (Figs. 6 and 7) should mainly be attributed to the creation of defects (interstitial atoms and vacancies) in the bulk of the AFM. We also irradiate pieces of the Ir-Mn/Fe(0.5 nm)/Co film using higher fluences (where defects at the FM-AFM interface could be more important) and observe further slow, gradual decays of both H_C and J_{eff}. The value of the latter after IB at 1×10^{16} ions/cm^2 is practically the same as for fluence 20 times lower (i.e., 5×10^{14} ions/cm^2).

F. Interface coupling versus SL thickness

Further proof that there is no important FM-AFM interface intermixing after IB in the Ir-Mn/Fe/Co structures is found in Fig. 8. It shows the $J_{eff}(t_{SL})$ variations estimated for all series after annealing, together with those corresponding to the fluences that yield the highest H_{EB} for the FM-spacer samples; the $J_{eff}(t_{Ru})$ curve for fluence of 1×10^{14} ions/cm^2 is also plotted. Again, since both $J_{Ir\text{-}Mn/Fe}$ and $J_{Ir\text{-}Mn/Py}$ are higher than $J_{Ir\text{-}Mn/Co}$, the initial rise of J_{eff} (130% and 90% for Fe and Py spacers, respectively) should be attributed to a coupling enhancement as the pinned Co atoms are replaced by Fe or Py (i.e., Ni and Fe). Once the Fe atoms cover all set-type UCSs, n_{set} ($\propto J_{eff}/J$) remains constant no matter what the thickness, $t_{Co} + t_{Fe}$, of the FM layer subsequently deposited is. This result is in agreement with the hypothesis that in polycrystalline films the pinning UCSs are located at grain boundaries on top of the AFM layer [45], so n_{set} should remain constant when this layer is deposited before the FM layer. None of our postdeposition treatments of the films with $t_{Fe} \geq 0.5$ nm changes significantly the pinning part of the FM-AFM interface.

As mentioned above, the M_S value of small-particle systems or very thin films might increase from zero (as a rule, exponentially) with increasing particle size or film thickness [46]. The variations of M_S of our SLs are unknown, so it is not *a priori* clear how these may influence the estimated J_{eff} values. The dashed lines in Fig. 8 give $J_{eff}(t_{SL})$ for the annealed films, where a linear increase (slower than an exponential one) from zero to 60% of the literature M_S values of each spacer is assumed. It is seen that such a trend of increase of M_S of the Py spacer does not practically affect $J_{eff}(t_{SL})$. For the other SL series, although a decrease of the thus-estimated J_{eff} is observed as compared with that for constant M_S for $t_{Fe} \geq 0.5$ nm, the greater difference is only approximately 10%. Even assuming that each SL is a magnetic dead layer [47] with zero M_S, we obtain a maximum difference in J_{eff} of 26% for the Fe spacer and 16% for the Py spacer. More importantly, the finding that $J_{eff}(t_{SL})$ is qualitatively the same for both constant or variable M_S of the SL supports the above statements concerning the dependencies of J_{eff} on IB fluence and t_{SL}.

G. The influence of interface roughness

The literature results on the influence of the interface roughness on the EB in polycrystalline FM-AFM layers are rather contradictory. While most investigations have led to the conclusion that H_{EB} decreases with

increasing roughness, some systems do not seem sensitive to the interfacial roughness and others show enhanced bias with increasing roughness (see, e.g., Refs. [48,49]). Co/Ir-Mn film interfaces were characterized by small-angle x-ray reflectivity, cross-section transmission electron microscopy, and nanobeam electron diffraction [50]. It was found that the interface roughnesses, before and after annealing, are practically identical. The same should hold for our films given that these are grown and annealed with the same facilities and in very similar manners.

As mentioned above, EB and H_C modifications of Ir-Mn/Co films with a moderate He^+ IB fluence as shown in Figs. 6 and 7 are mainly attributed to defect creation in the bulk of the AFM, and not to other effects such as increase of the interface roughness [10].

The variations of the EB parameters after annealing or IB of the Ru-spacer films (Figs. 4–8) support the considerations above. The nonmagnetic Ru spacer layer decreases the effective Co/Ir-Mn interaction and, from an interfacial coupling point of view, plays the opposite role when compared with both Py and Fe, since these have higher coupling (to Ir-Mn) values than Co. If the EB rise observed for the thinner FM spacers after annealing or IB is caused by an increase of the interface roughness, the Ru-spacer series should also show an initial H_{EB} enhancement; a steady decrease is seen instead. Although such a result does not prove that the roughness does not affect the EB parameters, it suggests that it is certainly not the main cause of the observed behavior. Also, the variations of J_{eff} and H_C with the IB fluence for the Ru-spacer series, even when a fluence 100 times higher is used (see Fig. 6), are rather insignificant as compared with those of the FM-spacer films.

H. Mechanisms determining the bias and coercivity variations

Remarkably, the variations with the fluence of J_{eff} (decreasing) and H_C (increasing) for the Py-spacer system (see Figs. 6 and 7) are completely opposite to those of Ir-Mn/Fe/Co. This indicates that for the Py spacer some other mechanism(s) should prevail over the hyperthermal heating and defect creation in the AFM (the latter should also exist in the Py-spacer films since the AFM layers, deposited before the rest of the magnetic layers, are practically identical for both systems).

The chief mechanisms that lead to the decrease of J_{eff} and to the enhancement of H_C in our Ir-Mn/Py/Co structures are, most probably, interdiffusion and defect creation at the FM-AFM interface. These effects seem typical for EB systems where Ni-Fe is used as the FM. It has been shown that in $Co_{80}Fe_{20}/Ir_{20}Mn_{80}$ and $Ni_{80}Fe_{20}/Ir_{20}Mn_{80}$ films the thermal diffusion of Mn atoms from the Ir-Mn layer into the adjacent Ni-Fe layer is much easier and faster than that into the Co-Fe layer [51]. Most specifically, given that use of low-nickel permalloy provides higher magnetic interface ordering and smaller Ir-Mn critical thickness to set the EB [52], the tendency of Mn to interdiffuse with Ni seems to be much greater than that for Mn-Fe interdiffusion. The Mn-Ni interdiffusion lowers the Ir-Mn anisotropy at the interface as t_{Py} is increased, reducing its pinning capacity and, therefore, the bias. The higher the fluence, the greater the Mn-Ni intermixing is, which explains why in Fig. 4 only $H_{EB}(t_{Py})$ for the IB where the lowest fluences (which cause low diffusion) are used shows maxima. This mechanism seems to be responsible for the decay of J_{eff} with t_{Py} as well (see Fig. 8) once the Py atoms have covered all already-existing set-type UCSs for $t_{Py} > 0.5$ nm, differently from the Fe-spacer case. The higher the degree of FM-AFM interface intermixing, the smaller n_{set} and, simultaneously, the higher n_{rot}. This also explains the enhancement of H_C with the fluence, especially for small t_{Py} values.

Intriguingly, the effects of He^+ IB with moderate (e.g., 1×10^{15} ions/cm^2 for the Fe-spacer films) to low (1×10^{13} ions/cm^2 for the Py-spacer films) fluences seem essentially identical to those produced by annealing since the respective $H_{EB}(t_{SL})$ and $J_{eff}(t_{SL})$ curves, shown in Figs. 4 and 8, are very similar. The same holds for $H_C(t_{SL})$ (see Fig. 5), the exception being the greater coercivity of the samples with $t_{SL} = 0.25$ and 0.5 nm after IB. This particular difference should be associated with the effects IB causes in interfaces where Fe, Ni, and Co atoms coexist. One possibility is that IB creates more Fe/Ir-Mn and Ni/Ir-Mn mixtures than the annealing and, subsequently, the more-efficient increase of n_{rot} of UCSs coupled to Fe and Ni. Having in mind that the $J_{Ir\text{-}Mn/Co}$ value is smaller than any of $J_{Ir\text{-}Mn/Fe}$ and $J_{Ir\text{-}Mn/Py}$ values [36,37], IB would cause faster enhancement of H_C than annealing.

The easy-axis hysteresis loops with the highest EB for the Ir-Mn/Fe(0.5 nm)/Co film obtained after either IB or annealing are shown in Figs. 1(c) and 1(e), respectively. It is noteworthy that although both curves exhibit practically the same H_{EB} values, H_C of the irradiated sample is approximately 3 times greater than that of the annealed sample. This demonstrates that one can fine-tune the values of the field shift and coercivity in EB systems by means of a proper postdeposition treatment.

IV. SUMMARY AND CONCLUSIONS

We report on exchange bias and coercivity modifications of either annealed or ion-irradiated Ir-Mn/SL/Co films (SL is Fe, Py, or Ru). XMCD results show the existence of small uncompensated Mn magnetization at the FM-AFM interface coupled, preferentially, antiferromagnetically to Fe moments. This suggests the formation of small FeMn interfacial clusters, which, as the rest of the Fe atoms at the interface, reverse their magnetizations together with those of Co and Ni.

Almost all $H_{EB}(t_{SL})$ variations for the series with FM spacers exhibit a significant initial rise (ascribed to an enhancement of J_{eff}) up to $t_{SL} \approx 0.5$ nm, followed by the normally expected monotonous decrease. $H_C(t_{SL})$ after annealing shows a general trend of decrease; the $H_C(t_{SL})$ versus t_{SL} curves of the irradiated samples are similar to $H_{EB}(t_{SL})$.

The variations of J_{eff} and H_C with the IB fluence of the two series of films with FM spacers are completely opposite. Gradual rise of J_{eff} and decrease of H_C for moderate fluences are observed for the Ir-Mn/Fe/Co films. The Py-spacer series, however, exhibits a steady decrease of J_{eff} and a general trend of coercivity enhancement.

While defect creation in the bulk of the AFM is mainly responsible for the changes of the EB characteristics of the Ir-Mn/Fe/Co films, the respective mechanisms for the Py-spacer series are interdiffusion and defect creation at the FM-AFM interface. The initial rise of J_{eff} is attributed to a coupling enhancement as the pinned Co atoms are replaced by Fe or Py.

None of the treatments of our films with $t_{Fe} \geq 0.5$ nm change significantly the pinning part of the FM-AFM interface. On the other hand, the tendency of Mn to interdiffuse with Ni seems much greater than that for interdiffusion with Fe, thus decreasing the Ir-Mn anisotropy at the interface as t_{Py} rises, lowering its pinning capacity and the bias. This mechanism is also responsible for the decay of J_{eff} with t_{Py}, differently from the Fe-spacer case.

The above conclusions are reinforced by the results for the Ru-spacer series.

Although the Ir-Mn/Fe(0.5 nm)/Co film shows the same maximum H_{EB} value after either IB or annealing, H_C after IB is approximately 3 times greater than after annealing. This demonstrates that, by proper postdeposition treatment, one can controllably tune the EB characteristics of such films.

In summary, the insertion of a very thin SL with $J_{Ir\text{-}Mn/SL} > J_{Ir\text{-}Mn/Co}$ at the Ir-Mn/Co interface strengthens substantially J_{eff} if the interfacial part of the AFM is unchanged (i.e., neither annealing nor IB produces important interdiffusion and/or defects). Otherwise, after an initial rise, J_{eff} decreases and H_C increases with t_{SL}. Although, strictly speaking, the reported results concern a particular system, they reveal mechanisms that are also important for other EB systems and materials, providing hints for understanding their behavior.

ACKNOWLEDGMENTS

We thank C. Deranlot and F. Petroff (UMP CNRS/Thales) for preparation of the films, and A.P.O. Bastos for his assistance in the annealing and AGFM measurements on the Ir-Mn/Ru/Co series. The ion bombardment was performed at LII, IF-UFRGS. This research was supported by the Brazilian agencies CNPq (Grant No. 305796/2016-0) and Coordenação de Aperfeiçoamento de Pessoal de Nível Superior (CAPES) (Finance Code 001). V.S. acknowledges financial support from the Spanish Ministry of Economy, Competitiveness and Universities through Projects No. MAT2015-71664-R and MAT2017-85232-R, and the European Union's FEDER program.

[1] W. H. Meiklejohn and C. P. Bean, New magnetic anisotropy, Phys. Rev. **102**, 1413 (1956); New magnetic anisotropy, *ibid.* **105**, 904 (1957).

[2] J. Schmalhorst, V. Höink, G. Reiss, D. Engel, D. Junk, A. Schindler, A. Ehresmann, and H. Schmoranzer, Influence of ion bombardment on transport properties and exchange bias in magnetic tunnel junctions, J. Appl. Phys. **94**, 5556 (2003).

[3] J. Fassbender and J. McCord, Magnetic patterning by means of ion irradiation and implantation, J. Magn. Magn. Mater. **320**, 579 (2008).

[4] D. Schafer, J. Geshev, S. Nicolodi, L. G. Pereira, J. E. Schmidt, and P. L. Grande, Controlled rotation of the exchange-bias direction in IrMn/Cu/Co via ion irradiation, Appl. Phys. Lett. **93**, 042501 (2008).

[5] J. Nogués, L. Morellon, C. Leighton, M. R. Ibarra, and I. K. Schuller, Antiferromagnetic spin flop and exchange bias, Phys. Rev. B **61**, 6455(R) (2000).; J. Nogués, J. Sort, S. Suriñach, J. S. Muñoz, M. D. Baró, J. F. Bobo, U. Lüders, E. Haanappel, M. R. Fitzsimmons, A. Hoffmann, and J. W. Cai, Isothermal tuning of exchange bias using pulsed fields, Appl. Phys. Lett. **82**, 3044 (2003).

[6] P. Miltényi, M. Gierlings, M. Bamming, U. May, G. Güntherodt, J. Nogués, M. Gruyters, C. Leighton, and I. K. Schuller, Tuning exchange bias, Appl. Phys. Lett. **75**, 2304 (1999).; N. J. Gökemeijer and C. L. Chien, Memory effects of exchange coupling in CoO/$Ni_{81}Fe_{19}$ bilayers, J. Appl. Phys. 85, 5516 (1999).; J. Geshev, L. G. Pereira, and V. Skumryev, Comment on Exchange bias dependence on interface spin alignment in a $Ni_{80}Fe_{20}$/(Ni,Fe)O thin film, Phys. Rev. Lett. **100**, 039701 (2008).

[7] E. Fulcomer and S. H. Charap, Thermal fluctuation aftereffect model for some systems with ferromagnetic-antiferromagnetic coupling, J. Appl. Phys. **43**, 4190 (1972).

[8] S. Soeya, M. Fuyama, S. Tadokoro, and T. Imagawa, NiO structure-exchange anisotropy relation in the $Ni_{81}Fe_{19}$/NiO films and thermal stability of its NiO film, J. Appl. Phys. **79**, 1604 (1996).

[9] G. Vallejo-Fernandez, L. E. Fernandez-Outon, and K. O'Grady, Antiferromagnetic grain volume effects in metallic polycrystalline exchange bias systems, J. Phys. D: Appl. Phys. **41**, 112001 (2008).

[10] D. Schafer, P. L. Grande, L. G. Pereira, and J. Geshev, Ion irradiation effects on the exchange bias in IrMn/Co films, J. Appl. Phys. **109**, 023905 (2011).

[11] N. D. Müglich, A. Gaul, M. Meyl, A. Ehresmann, G. Götz, G. Reiss, and T. Kuschel, Time-dependent rotatable magnetic anisotropy in polycrystalline exchange-bias systems: Dependence on grain-size distribution, Phys. Rev. B **94**, 184407 (2016).

[12] R. D. McMichael, M. D. Stiles, P. J. Chen, and W. F. Egelhoff, Jr., Ferromagnetic resonance studies of NiO-coupled thin films of $Ni_{80}Fe_{20}$, Phys. Rev. B **58**, 8605 (1998).

[13] J. Geshev, L. G. Pereira, and J. E. Schmidt, Rotatable anisotropy and coercivity in exchange-bias bilayers, Phys. Rev. B **66**, 134432 (2002).; J. Geshev, L. G. Pereira, J. E. Schmidt, L. C. C. M. Nagamine, E. B. Saitovitch, and F. Pelegrini, Frequency dependent exchange bias in NiFe/NiO films, Phys. Rev. B **67**, 132401 (2003).

[14] D. Schafer, P. L. Grande, L. G. Pereira, G. M. Azevedo, A. Harres, M. A. de Sousa, F. Pelegrini, and J. Geshev, Antiparallel interface coupling evidenced by negative rotatable anisotropy in IrMn/NiFe bilayers, J. Appl. Phys. **117**, 215301 (2015).

[15] S. Nicolodi, L. G. Pereira, A. Harres, G. M. Azevedo, J. E. Schmidt, I. García-Aguilar, N. M. Souza-Neto, C. Deranlot, F. Petroff, and J. Geshev, Negative rotatable anisotropy in IrMn/Cr/Co thin films, Phys. Rev. B **85**, 224438 (2012).

[16] A. Harres and J. Geshev, A polycrystalline model for magnetic exchange bias, J. Phys.: Condens. Matter **24**, 326004 (2012).

[17] T. Dias, E. Menéndez, H. Liu, C. Van Haesendonck, A. Vantomme, K. Temst, J. E. Schmidt, R. Giulian, and J. Geshev, Rotatable anisotropy driven training effects in exchange biased Co/CoO films, J. Appl. Phys. **115**, 243903 (2014).

[18] M. Ali, C. H. Marrows, and B. J. Hickey, Controlled enhancement or suppression of exchange biasing using impurity δ layers, Phys. Rev. B **77**, 134401 (2008).

[19] L. Thomas, A. J. Kellock, and S. S. P. Parkin, On the exchange biasing through a nonmagnetic spacer layer, J. Appl. Phys. **87**, 5061 (2000).

[20] F. Garcia, J. Sort, B. Rodmacq, S. Auffret, and B. Dieny, Large anomalous enhancement of perpendicular exchange bias by introduction of a nonmagnetic spacer between the ferromagnetic and antiferromagnetic layers, Appl. Phys. Lett. **79**, 3537 (2003).

[21] F. Ernult, B. Dieny, L. Billard, F. Lançon, and J. R. Regnard, Increase in ferromagnetic/antiferromagnetic exchange bias due to a reduction of the interfacial exchange interaction, J. Appl. Phys. **94**, 6678 (2003).

[22] S. Nicolodi, A. Harres, L. G. Pereira, J. E. Schmidt, M. A. de Sousa, F. Pelegrini, A. D. C. Viegas, C. Deranlot, F. Petroff, and J. Geshev, Abrupt suppression of the exchange bias across a non-magnetic insulator spacer, J. Appl. Phys. **110**, 063922 (2011).

[23] M. Tsunoda, S. Yoshitaki, Y. Ashizawa, D. Y. Kim, C. Mitsumata, and M. Takahashi, Enhancement of exchange bias by ultra-thin Mn layer insertion at the interface of Mn-Ir/Co-Fe bilayers, Phys. Stat. Sol. **244**, 4470 (2007).

[24] H. Endo, A. Hirohata, J. Sagar, L. R. Fleet, T. Nakayama, and K. O'Grady, Effect of interface structure on exchange biased Heusler alloy films, IEEE Trans. Magn. **48**, 2896 (2012).; R. Carpenter, N. C. Cramp, and K. O'Grady, Effect of Mn interface doping in polycrystalline exchange bias thin films, IEEE Trans. Magn. **48**, 4351 (2012).

[25] L. Lechevallier, A. Zarefy, R. Lardé, H. Chiron, J.-M. Le Breton, V. Baltz, B. Rodmacq, and B. Dieny, Structural analysis and magnetic properties of $(Pt/Co)_3/Pt_{tPt}$/IrMn multilayers, Phys. Rev. B **79**, 174434 (2009); A. Zarefy, L. Lechevallier, R. Lardé, H. Chiron, J.-M. Le Breton, V. Baltz, B. Rodmacq, and B. Dieny, Influence of Co layer thickness on the structural and magnetic properties of $(Pt/Co_{t_{Co}})_3/Pt_{t_{Pt}}$/IrMn multilayers, J. Phy. D: Appl. Phys. **43**, 215004 (2010).

[26] M. Tsunoda, H. Takahashi, T. Nakamura, C. Mitsumata, S. Isogami, and M. Takahashi, Linear correlation between uncompensated antiferromagnetic spins and exchange bias in Mn-Ir/$Co_{100-x}Fe_x$ bilayers, Appl. Phys. Lett. **97**, 072501 (2010).

[27] L. Klein, Comment on "Exchange bias-like phenomenon in SrRuO3" [Appl. Phys. Lett. 88, 102502 (2006)], Appl. Phys. Lett. **89**, 036101 (2006); J. Geshev, Comment on "Exchange bias and vertical shift in $CoFe_2O_4$ nanoparticles" [J. Magn. Magn. Mater. 313 (2007) 266], J. Magn. Magn. Mater. **320**, **600** (2008).; Comment on "Cluster glass induced exchange biaslike effect in the perovskite cobaltites" [Appl. Phys. Lett. 90, 162515 (2007)], J. Geshev, Appl. Phys. Lett. **93**, 176101 (2008).; Comment on 'Particle size dependent exchange bias and cluster-glass states in $LaMn_{0.7}Fe_{0.3}O_3$,' J. Geshev, J. Phys.: Condens. Matter **21**, 078001 (2009).

[28] A. Harres, M. Mikhov, V. Skumryev, A. M. H. de Andrade, J. E. Schmidt, and J. Geshev, Criteria for saturated magnetization loop, J. Magn. Magn. Mater. **402**, 76 (2016).

[29] A. Ehresmann, D. Junk, D. Engel, A. Paetzold, and K. Röll, On the origin of ion bombardment induced exchange bias modifications in polycrystalline layers, J. Phys. D **38**, 801 (2005).

[30] K. O'Grady, L. E. Fernandez-Outon, and G. Vallejo-Fernandez, A new paradigm for exchange bias in polycrystalline thin films, J. Magn. Magn. Mater. **322**, 883 (2010).

[31] A. E. Berkowitz, J.-I. Hong, S. K. McCall, E. Shipton, K. T. Chan, T. Leo, and D. J. Smith, Refining the exchange anisotropy paradigm: Magnetic and microstructural heterogeneity at the Permalloy-CoO interface, Phys. Rev. B **81**, 134404 (2010).

[32] E. C. Longhi, P. Bencok, A. Dobrynin, E. C. M. Rial, A. Rose, P. Steadman, C. Thompson, A. Thomson, and H. Wang, Developments in polarization and energy control of APPLE-II Undulators at Diamond Light Source, J. Phys.: Conf. Ser. **425**, 032011 (2013).

[33] H. Takahashi, Y. Kota, M. Tsunoda, T. Nakamura, K. Kodama, A. Sakuma, and M. Takahashi, Uncompensated antiferromagnetic moments in Mn-Ir/FM (FM = Ni-Co, Co-Fe, Fe-Ni) bilayers: Compositional dependence and its origin, J. Appl. Phys. **110**, 123920 (2011).

[34] J. Nogués and I. K. Schuller, Exchange bias, J. Magn. Magn. Mater. **192**, 203 (1999).

[35] H. Ohldag, A. Scholl, F. Nolting, E. Arenholz, S. Maat, A. T. Young, M. Carey, and J. Stöhr, Correlation between exchange bias and pinned interfacial spins, Phys. Rev. Lett. **91**, 017203 (2003).

[36] X. Yin, W. Sun, W. T. Soh, P. Yang, X. Yu, M. B. H. Breese, A. T. S. Weed, A. Rusydi, and C. K. Ong, Unraveling the magnetic coupling in the interface of the exchange-biased IrMn/permalloy multilayers, Mater. Lett. **187**, 133 (2017).

[37] M. Gamino, A. M. H. de Andrade, J. E. Schmidt, and J. Geshev, Strongly enhanced exchange bias of top-pinned

Co/IrMn films with Py spacers, J. Phy. D: Appl. Phys. **47**, 475001 (2014).

[38] D. V. Dimitrov, S. Zhang, J. Q. Xiao, G. C. Hadjipanayis, and C. Prados, Effect of exchange interactions at antiferromagnetic/ferromagnetic interfaces on exchange bias and coercivity, Phys. Rev. B **58**, 12090 (1998).

[39] S. Zhang, D. V. Dimitrov, G. C. Hadjipanayis, J. W. Cai, and C. L. Chien, Coercivity induced by random field at ferromagnetic and antiferromagnetic interfaces, J. Magn. Magn. Mater. **198-199**, 468 (1999).

[40] M. D. Stiles and R. D. McMichael, Coercivity in exchange-bias bilayers, Phys. Rev. B **63**, 064405 (2001).

[41] S. Poppe, J. Fassbender, and B. Hillebrands, On the mechanism of irradiation-enhanced exchange bias, Europhys. Lett. **66**, 430 (2004).

[42] A. Ehresmann, He-ion bombardment induced exchange bias modifications: Fundamentals and applications, Recent Res. Dev. Appl. Phys. **7**, 401 (2004).

[43] D. Engel, A. Ehresmann, J. Schmalhorst, M. Sacher, V. Höink, and G. Reiss, Initialization of unidirectional anisotropy in a ferromagnet-antiferromagnet bilayer by keV-He ion bombardment, J. Magn. Magn. Mater. **293**, 849 (2005).

[44] N. D. Müglich, M. Merkel, A. Gaul, M. Meyl, G. Götz, G. Reiss, T. Kuschel, and A. Ehresmann, Preferential weakening of rotational magnetic anisotropy by keV-He ion bombardment in polycrystalline exchange bias layer systems, New J. Phys. **20**, 053018 (2018).

[45] H. Ohldag, H. Shi, E. Arenholz, J. Stöhr, and D. Lederman, Parallel versus antiparallel interfacial coupling in exchange biased Co/FeF_2, Phys. Rev. Lett. **96**, 027203 (2006).

[46] A. E. Berkowitz, W. J. Schuele, and P. J. Flanders, Influence of crystallite size on the magnetic properties of acicular $\gamma-Fe_2O_3$ particles, J. Appl. Phys. **39**, 1261 (1968).

[47] L. N. Liebermann, D. R. Fredkin, and H. B. Shore, Two-dimensional "ferromagnetism" in iron, Phys. Rev. Lett. **22**, 539 (1969); W. Göpel, "Magnetic dead layers" on chemisorption at ferromagnetic surfaces, Surf. Sci. **85**, 400 (1979).

[48] C. Fleischmann, F. Almeida, J. Demeter, K. Paredis, A. Teichert, R. Steitz, S. Brems, B. Opperdoes, C. Van Haesendonck, A. Vantomme, and K. Temst, The influence of interface roughness on the magnetic properties of exchange biased CoO/Fe thin films, J. Appl. Phys. **107**, 113907 (2010).

[49] M. Vafaee, S. Finizio, H. Deniz, D. Hesse, H. Zabel, G. Jakob, and M. Klaui, The effect of interface roughness on exchange bias in $La_{0.7}Sr_{0.3}MnO_3-BiFeO_3$ heterostructures, Appl. Phys. Lett. **108**, 072401 (2016).

[50] J. Geshev, T. Dias, S. Nicolodi, R. Cichelero, A. Harres, J. J. S. Acuña, L. G. Pereira, J. E. Schmidt, C. Deranlot, and F. Petroff, Role of the uncompensated interface spins in polycrystalline exchange-biased systems, J. Phys. D: Appl. Phys. **44**, 095002 (2011).

[51] Y. D. Kim, K. S. Yoon, J. H. Koo, K. W. Kim, C. O. Kim, and J. P. Hong, Enhanced exchange bias and thermal stability of magnetic tunnel junctions with Ta blocking layer, J. Korean Phys. Soc. **45**, 683 (2004).

[52] I. O. Dzhun, G. V. Babaytsev, N. G. Chechenin, C. A. Gritsenko, and V. V. Rodionova, FMR investigations of exchange biased NiFe/IrMn/NiFe trilayers with high and low Ni relative content, J. Magn. Magn. Mater. **470**, 151 (2019).